

Precision Characterization of the $^2D_{5/2}$ State and Quadratic Zeeman Coefficient in $^{171}\text{Yb}^+$

T. R. Tan,^{1,*} C. L. Edmunds,² A. R. Milne,² M. J. Biercuk,² and C. Hempel^{2,3,†}

¹The University of Sydney, School of Physics, NSW, 2006, Australia

²ARC Centre of Excellence for Engineered Quantum Systems,
The University of Sydney, School of Physics, NSW, 2006, Australia

³The University of Sydney Nano Institute (Sydney Nano),
The University of Sydney, NSW 2006, Australia

(Dated: Tuesday 28th June, 2022)

We report measurements of the branching fraction, hyperfine constant, and second-order Zeeman coefficient of the $^2D_{5/2}$ level in $^{171}\text{Yb}^+$ with up to two orders-of-magnitude improvement in precision compared to previously reported values. We estimate the electric quadrupole reduced matrix element of the $^2S_{1/2} \leftrightarrow ^2D_{5/2}$ transition to be $12.5(4) ea_0^2$. Furthermore, we determine the transition frequency of the $^2F_{7/2} \leftrightarrow ^1D[3/2]_{3/2}$ at 760 nm with a ~ 25 -fold improvement in precision. These measurements provide essential benchmarks for quantum-many-body atomic-physics calculations and provide valuable data for efforts to improve quantum information processors based on $^{171}\text{Yb}^+$.

Trapped atomic ions combine the benefits of long storage time and excellent isolation from the environment, providing an attractive physical system for numerous applications in quantum technology [1, 2]. Among the singly-charged ions most commonly investigated, $^{171}\text{Yb}^+$ has found applications in tests of fundamental physics [3, 4], frequency metrology [5, 6], and quantum information processing (QIP) [7–10]. All of these applications rely on a deep understanding of atomic structure theory, which is guided by and refined through precision measurements [11–17]. However, accurate calculation of the atomic properties for $^{171}\text{Yb}^+$ has proven to be highly challenging due to its large number of valence electrons and complications arising from mixing between electronic configurations [14], making it a particularly interesting system for experimental investigation.

The nuclear spin of $^{171}\text{Yb}^+$ is one half, causing the $^2S_{1/2}$ electronic ground state to split into a hyperfine doublet separated by ~ 12.64 GHz. Its metastable levels (Fig. 1) include $^2D_{3/2}$, $^2D_{5/2}$, and $^2F_{7/2}$ with lifetimes of 52.7 ms [18], 7.2 ms [19], and $\gtrsim 5.4$ years [20], respectively. The short lifetime of $^2D_{5/2}$ has made the state less attractive for frequency metrology compared to $^2D_{3/2}$ [21, 22] and $^2F_{7/2}$ [5, 23, 24]; experimental measurements on $^2D_{5/2}$ were last reported more than 20 years ago [25]. Nonetheless the $^2S_{1/2} \leftrightarrow ^2D_{5/2}$ electric quadrupole (E2) transition is a potential candidate for probing nuclear-spin-dependent parity non-conservation (PNC) and nuclear anapole moments as a relatively inexpensive, low-energy test of the standard model when compared to high-energy searches using massive accelerators [13, 14, 17, 26, 27]. These investigations compare experimentally measured atomic PNC with predictions from atomic many-body calculations. Specifically, precision measurements of atomic properties such as reduced

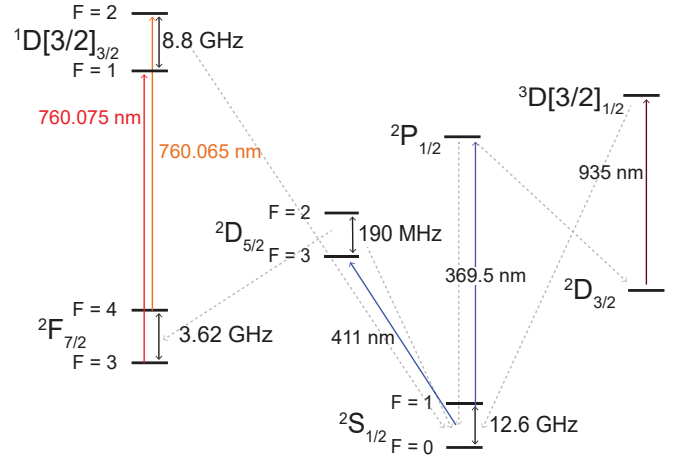


FIG. 1. Selected energy levels and transition wavelengths in $^{171}\text{Yb}^+$. Dashed lines show relevant decay channels. Our work focuses on the 411 nm electric quadrupole (E2) $^2S_{1/2} \leftrightarrow ^2D_{5/2}$ transition. The $^2D_{5/2} |F=3\rangle$ decays to $^2S_{1/2} |F=1\rangle$ and $^2F_{7/2} |F=3, 4\rangle$ and $^2D_{5/2} |F=2\rangle$ decays to $^2S_{1/2} |F=0, 1\rangle$ and $^2F_{7/2} |F=3\rangle$. A 760 nm laser is used for fast repumping of $^2F_{7/2}$ to $^2S_{1/2}$ via $^1D[3/2]_{3/2}$. Some hyperfine structures and Zeeman sublevels are omitted for clarity.

matrix elements, g -factors, lifetimes and branching ratios provide necessary and complementary input parameters for high accuracy tests. In addition to testing fundamental physics and providing benchmarks for atomic calculations, the metastable 2D levels in $^{171}\text{Yb}^+$ provide extra degrees of freedom for applications in QIP. These find use in implementing entangling gate operations [28] or to scalably improving qubit measurement fidelities with minimal technical overhead [29].

In this Letter, we report precision measurements on branching ratios, the quadratic Zeeman (QZ) coefficient, and the hyperfine splitting of the $^2D_{5/2}$ state in $^{171}\text{Yb}^+$, with precision up to two order of magnitude higher than

* tingrei86@gmail.com

† cornelius.hempel@gmail.com

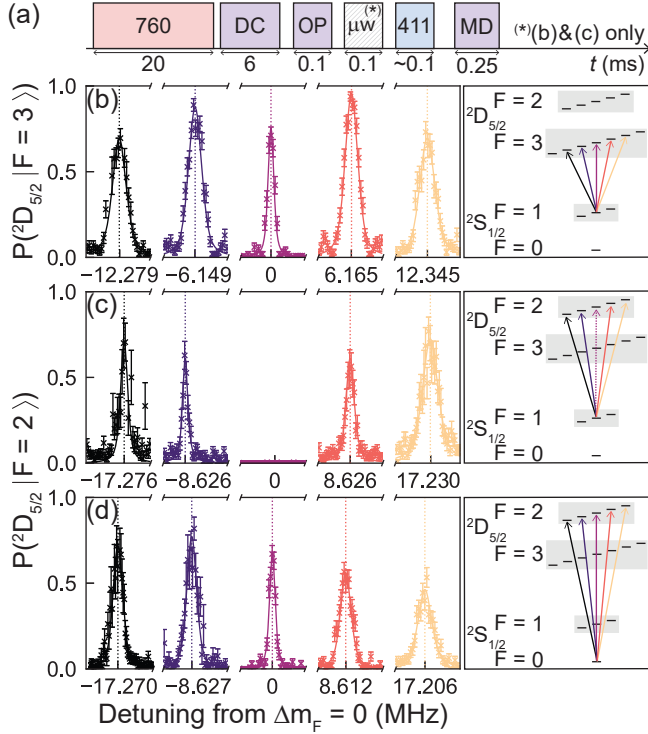


FIG. 2. Spectra of the $^2S_{1/2} \leftrightarrow ^2D_{5/2}$ transitions at 411 nm. (a) The spectroscopy pulse sequence including 760 nm repumping, Doppler cooling (DC), optical pumping to prepare $^2S_{1/2} |F=0, m_F=0\rangle$ (OP), microwave excitation to $^2S_{1/2} |F=1, m_F=0\rangle$ in select cases (μW), the 411 nm spectroscopy pulse and detection (MD), which includes the same frequency components as DC but is tuned closer to resonance. (b,c,d) 411 nm laser frequency scans around the line center at $\Delta m_F = 0$ for the different hyperfine transitions indicated in corresponding colors on the right. In (c), the $\Delta m_F = 0$ transition cannot be driven due to atomic selection rules. Error bars are calculated from quantum projection noise (QPN) and the data are fitted to Voigt profiles. The precision of the indicated center frequencies is limited by the fitting error to (0.1-2) kHz; amplitude differences are due to polarization and beam orientation with respect to the quantization axis.

the previous best reported values. Our spectroscopic experiments use a single ion in a Paul trap with a storage lifetime of several months, and a new stabilized solid-state laser near 411 nm. Furthermore, we provide a more precise measurement of the transition between $^2F_{7/2} \leftrightarrow ^1D[3/2]_{3/2}$ at 760 nm than previously reported [30–32].

The experimental setup is detailed in Ref. [33]. A permanent magnet produces a quantization field of ~ 0.44 mT at the ion position, which we infer using the 13.98(1) GHz/T linear Zeeman shift of the $^2S_{1/2}$ stretched states [34, 35]. A 369.5 nm laser in conjunction with electro-optic modulators (EOMs) is used for Doppler cooling, state preparation, and detection. Separate 369 nm laser beamlines allow for selective measurements of just the population in $^2S_{1/2} |F=1\rangle$ using the

“standard detection” (SD), or the entire $^2S_{1/2}$ “manifold detection” (MD). A 935 nm laser continuously repumps population which has decayed into the $^2D_{3/2}$ manifold.

We drive the $^2S_{1/2} \leftrightarrow ^2D_{5/2}$ transition using an external-cavity diode laser at 411 nm, which is locked to an ultra-low expansion reference cavity with a free spectral range (FSR) of 1.5 GHz, a finesse of approximately 32,000, and a frequency drift rate of ~ 320 mHz/s. An additional, cavity-stabilized 760 nm cat-eye diode laser is used to provide efficient repumping from the long-lived $^2F_{7/2}$ via $^3D[3/2]_{1/2}$, which has a lifetime of ~ 28.6 ns and decays primarily to the $^2S_{1/2}$ ground states [30, 36]. To maximise repumping efficiency, an EOM driven at 5.258 GHz is used to create an additional laser frequency component, matching the hyperfine splittings of 3.620 GHz [37, 38] and 8.8 GHz [32] for $^2F_{7/2}$ and $^1D[3/2]_{3/2}$, respectively. With an intensity of ~ 630 kW/m², the typical repumping time from the $^2F_{7/2}$ state to the $^2S_{1/2}$ manifold is ~ 20 ms, significantly faster than other repumping channels [18, 19, 30, 39, 40], such as the 638 nm transition to $^1D[5/2]_{5/2}$. All laser beams are controlled by acousto-optic modulators driven by direct digital synthesis sources referenced to a rubidium frequency standard.

We begin by performing spectroscopy on the $^2S_{1/2} \leftrightarrow ^2D_{5/2}$ optical transition near 411 nm, resolving individual hyperfine and Zeeman levels as shown in Figure 2. The ion is initialized in $^2S_{1/2} |F=0, m_F=0\rangle$ by optical pumping and optionally transferred to $^2S_{1/2} |F=1, m_F=0\rangle$ through application of a microwave π -pulse. After applying a 411 nm spectroscopy pulse of fixed duration, state-dependent fluorescence is induced by a 369 nm (MD) pulse that distinguishes population in the $^2S_{1/2}$ manifold (“bright”) from that in other levels (“dark”). A 20 ms pulse at 760 nm is applied to repump population decayed to $^2F_{7/2}$ at the beginning of each measurement cycle. The center frequency for each transition is extracted by fitting the spectroscopic peaks to Voigt profiles. We measure a frequency of 729.487 752(178) THz, with an uncertainty limited by our wavemeter’s absolute accuracy, for the $^2S_{1/2} |F=0, m_F=0\rangle \leftrightarrow ^2D_{5/2} |F=2, m_F=0\rangle$ transition, consistent with previous measurements [25, 41].

The lifetimes and decay branching ratios of $^2D_{5/2}$ are measured by a sequence that initializes in $^2D_{5/2} |F=2\rangle$ or $^2D_{5/2} |F=3\rangle$ through multiple sequential π pulses to different Zeeman sublevels, followed by an immediate detection used for post selection on events with successful transfer. Following a variable wait time, two final detection pulses determine the population in the $^2S_{1/2}$ states and shelved manifolds (Fig. 3(a)). The lifetime is extracted by fitting exponential decays, weighed by QPN, to time-delayed data (Fig. 3(b,c)), where we take the asymptotic limits of the fit as branching ratios. This is the first $^2D_{5/2}$ lifetime and branching fraction measurement made on $^{171}\text{Yb}^+$. The values agree with previous measurements on different isotopes which we summarize

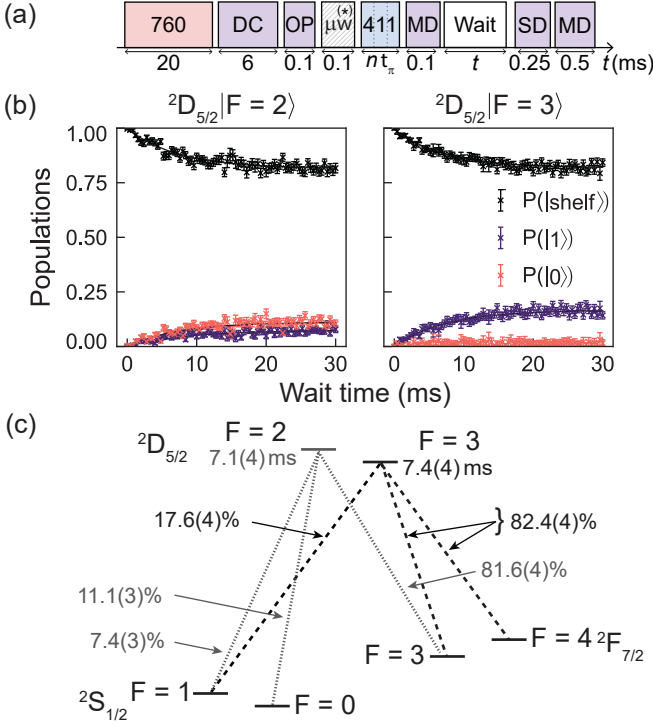


FIG. 3. Lifetime and branching ratio measurements. (a) Measurement pulse sequence similar to Fig. 2(a), with an added variable wait time t , surrounded by MD and detection pulses (SD and MD) for post selection and measurement of branching to the two $^2S_{1/2}$ levels, respectively. A series of $n = 5$ π pulses on the accessible 411 nm transitions to different Zeeman sublevels maximizes the shelving success to $^2D_{5/2} |F=2\rangle$. Due to the similar Zeeman splitting in $^2S_{1/2} |F=1\rangle$ and $^2D_{5/2} |F=3\rangle$ manifolds, a similar $n = 3$ procedure is used to prepare $^2D_{5/2} |F=3\rangle$ from $^2S_{1/2} |F=1, m_F=0\rangle$. (b) State decay curves as a function of wait time after initialization of the target state. The populations $P(|0\rangle)$ and $P(|1\rangle)$ refer to the two hyperfine levels in the $^2S_{1/2}$ ground state manifold, while $P(|shelf\rangle)$ refers to the shelved population in $^2D_{5/2}$ or $^2F_{7/2}$ which we deduce by $1 - P(|0\rangle) - P(|1\rangle)$. (c) Overview of the decay channels and branching fractions measured in this work.

in Table I. The asymptotic limits for the $|F=0\rangle$ and $|F=1\rangle$ populations are 11.1(3)% and 7.4(3)%, which agree well with expected Clebsch-Gordon coefficients. From the lifetime and branching ratios, we revise the estimate of the E2 reduced matrix element to be $12.5(4) ea_0^2$ where e and a_0 are the elementary electronic charge and Bohr radius, respectively, which is consistent with theoretical predictions [13, 43].

To deduce the second-order Zeeman coefficient of the $^2D_{5/2} |F=3, m_F=0\rangle$ state, we vary the magnetic field at the ion location over an interval of $\sim [0.44, 1]$ mT through adjustment of a permanent magnet's placement. For each B-field configuration, the frequencies of the $^2S_{1/2} |F=0, m_F=0\rangle \leftrightarrow ^2S_{1/2} |F=1, m_F=0\rangle$ hyperfine transition at ~ 12.6 GHz

	Decay to $^2S_{1/2}$	Decay to $^2F_{7/2}$	Lifetime (ms)
This work (exp.) $^{171}\text{Yb}^+ F=3\rangle$	17.6(4)%	82.4(4)%	7.1(4)
This work (exp.) $^{171}\text{Yb}^+ F=2\rangle$	18.4(4)%	81.6(4)%	7.4(4)
Taylor et al. [19] (1997 exp.) $^{172}\text{Yb}^+$	17(4)%	83(3)%	7.2(3)
Yu et al. [18] (2000 exp.) $^{174}\text{Yb}^+$	-	-	7.0(4)
Fawcett et al. [11] (1991 calc.) Yb II	19.7%	80.3%	5.74

TABLE I. Branching fractions and lifetimes for the $^2D_{5/2} |F=2, 3\rangle$ state contrasted with previous measurements and a theoretical prediction. Branching fraction to $^2F_{7/2}$ is deduced from $P(|shelf\rangle)$ described in Fig. 3. Uncertainties of 1σ are derived from exponential fits to the state evolution shown in Fig. 3.

and the $^2S_{1/2} |F=1, m_F=0\rangle \leftrightarrow ^2D_{5/2} |F=3, m_F=0\rangle$ transition at 411 nm are recorded, updated, and averaged through interleaved Ramsey interrogations using wait times of 50 ms and 0.1 ms, respectively. We compensate the measured optical frequencies for cavity drift and plot the ratio of the transitions' relative shift in Fig. 4. A linear fit yields a slope of $-11.27(4)$ where the uncertainty is the standard error of the fit. Taken together with the often quoted value of $0.03108 \text{ Hz}/\mu\text{T}^2$ [44] for the quadratic Zeeman coefficient in the $^2S_{1/2}$ ground state, this yields a QZ coefficient of $-0.350(1) \text{ Hz}/\mu\text{T}^2$ for $^2D_{5/2}$. This value is approximately an order of magnitude more precise than the best previously published result of $0.38(8) \text{ Hz}/\mu\text{T}^2$ measured on $^2S_{1/2} |F=0, m_F=0\rangle \leftrightarrow ^2D_{5/2} |F=2, m_F=0\rangle$ [20]. From the coefficient ratio measurement we can also deduce a Landé g -factor ratio of $0.582(6)$, which deviates from the $g_D/g_S = 1.202/1.998 = 0.602(3)$ given by Meggers [35].

The hyperfine splitting of $^2D_{5/2}$ can be deduced from the difference of the transition frequencies between $^2S_{1/2} |F=1, m_F=0\rangle$ and $^2D_{5/2} |F=2, m_F=0\rangle$ as well as $^2D_{5/2} |F=3, m_F=0\rangle$. Electric quadrupole transition selection rules forbid the $^2S_{1/2} |F=1, m_F=0\rangle \leftrightarrow ^2D_{5/2} |F=2, m_F=0\rangle$ transition to be directly driven; therefore we infer its value from measurements of $^2S_{1/2} |F=1, m_F=0\rangle \leftrightarrow ^2D_{5/2} |F=2, m_F=\pm 1\rangle$. The frequency of the 411 nm laser is stabilized to the same cavity mode throughout this measurement in order to avoid uncertainties from wavemeter's accuracy or cavity's FSR in the determination of hyperfine splitting. All transition frequencies are corrected for cavity drift over the measurement duration of ~ 4 hours and

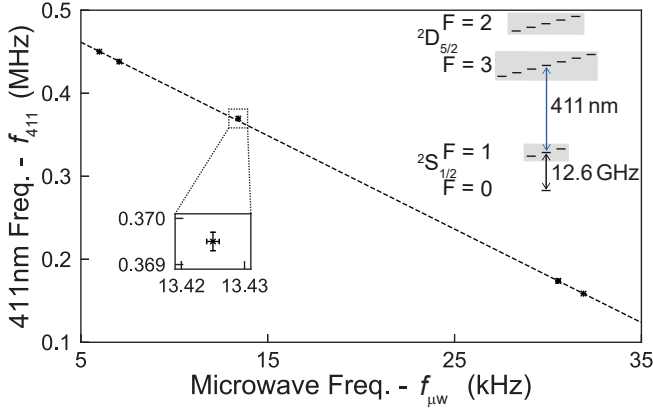


FIG. 4. Frequency of the $^2S_{1/2} |F=1, m_F=0\rangle \leftrightarrow ^2D_{5/2} |F=3, m_F=0\rangle$ 411 nm transition vs. the $^2S_{1/2} |F=0, m_F=0\rangle \leftrightarrow ^2S_{1/2} |F=1, m_F=0\rangle$ hyperfine transition at different magnetic field strengths. The corresponding transitions are illustrated on the right. Typical statistical uncertainties of the relative frequency measurements are approximately 200 Hz and 0.2 Hz for the optical and microwave frequencies, respectively, with the error bar size highlighted in the lower inset. The frequency offsets are $f_{\mu w} = 12.642812118466$ GHz, and $f_{411} = 729.487559$ THz.

QZ shifts at the B-field of $441.26(2)$ μT [42]. From our measurements we extract a hyperfine splitting of $-190.104(3)$ MHz and, correspondingly, a hyperfine constant of $A_{D,5/2} = -63.368(1)$ MHz. This measurement is more than two orders of magnitude more precise than the best previously reported value of $-191(2)$ MHz [25], and limited by the precision of the QZ coefficients and fitting errors. Table II summarizes both measured and theoretical values for $A_{D,5/2}$, illustrating the difficulty of performing exact calculations for $^{171}\text{Yb}^+$.

As a final measurement, we determine the $^2F_{7/2} \leftrightarrow ^1D[3/2]_{3/2}$ transition near 760 nm, used to repump population to $^2S_{1/2}$. We first prepare population in $^2D_{5/2} |F=2, 3, m_F=0\rangle$ using a 411 nm laser pulse, followed by a 10 ms wait time to allow population decay to $^2F_{7/2}$. A subsequent brief application of the 369 nm MD beam allows us to remove instances of $^2S_{1/2}$ decay

Reference	$A_{D,5/2}$ (MHz)
This work (2020 experiment)	-63.368(1)
Roberts et al. [25] (1999 experiment)	-63.6(7)
Nandy et al. [16] (2014 calculation)	-69(6)
Porsev et al. [14] (2012 calculation)	-96
Sahoo et al. [13] (2011 calculation)	-48(15)
Itano [12] (2006 calculation)	-12.58

TABLE II. Comparison of measurements and calculations of the $^2D_{5/2}$ hyperfine constant.

from the data in post processing. A 760 nm laser pulse is then applied to induce a transition to the short-lived $^1D[3/2]_{3/2}$ level, which primarily decays to $^2S_{1/2}$. Successful repump events then yield fluorescence under application of the 369 nm MD light. The measured center frequencies are

$$^2F_{7/2} |F=3\rangle \leftrightarrow ^1D[3/2]_{3/2} |F=1\rangle : 394.424\,943(20)\text{THz},$$

$$^2F_{7/2} |F=4\rangle \leftrightarrow ^1D[3/2]_{3/2} |F=2\rangle : 394.430\,203(16)\text{THz},$$

respectively. Here the uncertainties are dominated by line broadening due to our inability to prepare the ion in a specific $^2F_{7/2}$ Zeeman level and the wavemeter's specified absolute accuracy. These measurements improve precision by 25-fold over previously reported values [32].

In conclusion, we report measurements of the hyperfine splitting and branching ratios of $^2D_{5/2}$ in $^{171}\text{Yb}^+$ with improved precision and investigate the 760 nm transition to efficiently depopulate the $^2F_{7/2}$ state. These results can be used to benchmark and verify quantum many-body calculations and provide the necessary characterizations for improving measurement fidelity of $^{171}\text{Yb}^+$ qubits as detailed in Ref. [29].

We also report a precision measurement of the ratio of the second-order Zeeman coefficients of the $^2D_{5/2}$ metastable and $^2S_{1/2}$ ground state. Our ratio estimate disagrees with that determined from literature values last reported in 1967 [35]. Our measurements notwithstanding, we note that Meggers' ground state g -factor value of $1.998(2)$ implies a g -factor anomaly correction of -4×10^{-3} which is of opposite sign to the $\delta g = +79.8 \times 10^{-5}$ reported in Ref. [15]. Given the discrepancy and the importance of g -factors in the evaluation of magnetic field related systematic effects, *e.g.* in atomic frequency standards [34], a new measurement of the ground state Landé g -factor is needed. This could be measured in a Paul trap with a second co-trapped ion species. For example, one might consider employing $^{171}\text{Yb}^+$ simultaneously trapped with a Ba^+ ion [*e.g.* 45–47], as the g -factor of the latter has been previously determined with high precision [48, 49]. The most relevant systematic error in measuring the g -factor in such a scenario would arise from a potential magnetic field gradient between the ions, which could readily be calibrated through spectroscopy on different Zeeman levels and compensated through external fields to high precision, *e.g.* using correlation spectroscopy [50–52]. It is also possible to measure the $^{171}\text{Yb}^+$ g -factor in a Penning trap where the B-field magnitude can be independently determined via cyclotron motion [53].

ACKNOWLEDGEMENTS

T.R. Tan acknowledges support from the Sydney Quantum Academy. The authors thank A. Singh and T.F. Wohlers-Reichel for their contribution to assembling and maintenance of the experimental setup.

This work was partially supported by the Intelligence Advanced Research Projects Activity Grant No. W911NF-16-1-0070, the US Army Research Office Grant No. W911NF-14-1-0682, the Australian Research Council Centre of Excellence for Engineered Quantum

Systems Grant No. CE170100009, and a private grant from H.&A. Harley.

TRT and CE contributed equally to this work.

-
- [1] D. J. Wineland, C. Monroe, W. M. Itano, D. Leibfried, B. E. King, and D. M. Meekhof, “Experimental issues in coherent quantum-state manipulation of trapped atomic ions,” *Journal of Research of the National Institute of Standards and Technology*, **103**, 259 (1998).
 - [2] M. Knoop, L. Hilico, and J. Eschner, “Modern applications of trapped ions,” *Journal of Physics B: Atomic, Molecular and Optical Physics*, **42**, 150201 (2009).
 - [3] V. V. Flambaum, A. J. Geddes, and A. V. Viatkina, “Isotope shift, nonlinearity of King plots, and the search for new particles,” *Phys. Rev. A* **97**, 032510 (2018).
 - [4] I. Counts, J. Hur, D. P. L. Aude Craik, H. Jeon, C. Leung, J. C. Berengut, A. Geddes, A. Kawasaki, W. Jhe, V. Vuletić, “Evidence for Nonlinear Isotope Shift in Yb^+ Search for New Boson,” *Phys. Rev. Lett.* **125**, 123002 (2020).
 - [5] N. Huntemann, C. Sanner, B. Lipphardt, Chr. Tamm, and E. Peik, “Single-Ion Atomic Clock with 3×10^{-18} Systematic Uncertainty,” *Phys. Rev. Lett.* **116**, 063001 (2016).
 - [6] P. T. H. Fisk, M. J. Sellars, M. A. Lawn, and G. Coles, “Accurate measurement of the 12.6 GHz “clock” transition in trapped $^{171}\text{Yb}^+$ ions,” *IEEE Transactions on Ultrasonics, Ferroelectrics and Frequency Control* **44**, 344 (1997).
 - [7] A. Soare, H. Ball, H. D. Hayes, D. J. Sastrawan, M. C. Jarratt, J. J. McLoughlin, X. Zhen, T. J. Green, and M. J. Biercuk, “Experimental noise filtering by quantum control,” *Nature Physics* **10**, 825 (2014).
 - [8] S. Olmschenk, K. C. Younge, D. L. Moehring, D. Matsukevich, P. Maunz, and C. Monroe, “Manipulation and detection of a trapped Yb^+ hyperfine qubit,” *Phys. Rev. A* **76**, 052314 (2007).
 - [9] S. Mavadia, C. L. Edmunds, C. Hempel, H. Ball, F. Roy, T. M. Stace, and M. J. Biercuk, “Experimental quantum verification in the presence of temporally correlated noise,” *NPJ Quantum Inf.* **4**, 7 (2018).
 - [10] C. Monroe, W. C. Campbell, L.-M. Duan, Z.-X. Gong, A. V. Gorshkov, P. Hess, R. Islam, K. Kim, G. Pagano, P. Richerme, C. Senko, C. and N. Y. Yao, “Programmable Quantum Simulations of Spin Systems with Trapped Ions,” *arXiv:1912.07845*.
 - [11] B. C. Fawcett and M. Wilson, “Computed oscillator strengths, Landé g values, and lifetimes in Yb II ,” *Atomic Data and Nuclear Data Tables* **47**, 241 (1991).
 - [12] Wayne M. Itano, “Quadrupole moments and hyperfine constants of metastable states of Ca^+ , Sr^+ , Ba^+ , Yb^+ , Hg^+ , and Au ,” *Phys. Rev. A* **73**, 022510 (2006).
 - [13] B. K. Sahoo and B. P. Das, “Parity nonconservation in ytterbium ion,” *Phys. Rev. A* **84**, 010502(R) (2011).
 - [14] S. G. Porsev, M. S. Safronova, and M. G. Kozlov, “Correlation effects in Yb^+ and implications for parity violation,” *Phys. Rev. A* **86**, 022504 (2012).
 - [15] G. H. Gossel, V. A. Dzuba, and V. V. Flambaum, “Calculation of strongly forbidden M1 transitions and g-factor anomalies in atoms considered for parity-nonconservation measurements,” *Phys. Rev. A* **88**, 034501 (2013).
 - [16] D. K. Nandy and B. K. Sahoo, “Quadrupole shifts for the $^{171}\text{Yb}^+$ ion clocks: Experiments versus theories,” *Phys. Rev. A* **90**, 050503(R) (2014).
 - [17] B. M. Roberts, V. A. Dzuba, and V. V. Flambaum, “Nuclear-spin-dependent parity nonconservation in s-d $_{5/2}$ and s-d $_{3/2}$ transitions,” *Phys. Rev. A* **89**, 012502 (2014).
 - [18] N. Yu, and L. Maleki, “Lifetime measurements of the $4f^{14}5d$ metastable states in single ytterbium ions,” *Phys. Rev. A* **61**, 022507 (2000).
 - [19] P. Taylor, M. Roberts, S. V. Gateva-Kostova, R. B. M. Clarke, G. P. Barwood, W. R. C. Rowley, and P. Gill, “Investigation of the $^2S_{1/2}-^2D_{5/2}$ clock transition in a single ytterbium ion,” *Phys. Rev. A* **56**, 2699 (1997).
 - [20] M. Roberts, P. Taylor, G. P. Barwood, W. R. C. Rowley, and P. Gill, “Observation of the $2S_{1/2}-2F_{7/2}$ electric octupole transition in a single $^{171}\text{Yb}^+$ ion,” *Phys. Rev. A* **62**, 020501(R) (2000).
 - [21] S. Webster, R. Godun, S. King, G. Huang, B. Walton, V. Tsaturian, H. Margolis, S. Lea, and P. Gill, “Frequency measurement of the $^2S_{1/2}-^2D_{3/2}$ electric quadrupole transition in a single $^{171}\text{Yb}^+$ ion,” *IEEE Transactions on Ultrasonics, Ferroelectrics and Frequency Control* **57**, 592 (2010).
 - [22] M. Schacht, J. R. Danielson, S. Rahaman, J. R. Torgerson, J. Zhang, and M. M. Schauer, M M, “ $^{171}\text{Yb}^+ 5D_{3/2}$ hyperfine state detection and $F = 2$ lifetime,” *Journal of Physics B: Atomic, Molecular and Optical Physics*, **48**, 065003, (2015).
 - [23] K. Hosaka, S. A. Webster, A. Stannard, B. R. Walton, H. S. Margolis, and P. Gill, “Frequency measurement of the $^2S_{1/2}-^2F_{7/2}$ electric octupole transition in a single $^{171}\text{Yb}^+$ ion,” *Phys. Rev. A* **79**, 033403 (2009).
 - [24] Chr. Tamm, N. Huntemann, B. Lipphardt, V. Gerginov, N. Nemitz, M. Kazda, S. Weyers, and E. Peik, “Cs-based optical frequency measurement using cross-linked optical and microwave oscillators,” *Phys. Rev. A* **89**, 023820 (2014).
 - [25] M. Roberts, P. Taylor, S. V. Gateva-Kostova, R. B. M. Clarke, W. R. C. Rowley, and P. Gill, “Measurement of the $^2S_{1/2}-^2D_{5/2}$ clock transition in a single $^{171}\text{Yb}^+$ ion,” *Phys. Rev. A* **60**, 2867 (1999).
 - [26] W. C. Haxton, “Atomic Parity Violation and the Nuclear Anapole Moment,” *Science* **275**, 1753 (1997).
 - [27] C. S. Wood, S. C. Bennett, D. Cho, B. P. Masterson, J. L. Roberts, C. E. Tanner, and C. E. Wieman, “Measurement of Parity Nonconservation and an Anapole Moment in Cesium,” *Science* **275**, 1759 (1997).
 - [28] C. H. Baldwin, B. J. Bjork, M. Foss-Feig, J. P. Gaebler, D. Hayes, M. G. Kokish, C. Langer, J. A. Sedlacek, D. Stack, and G. Vittorini, “A high fidelity light-shift gate

- for clock-state qubits,” arXiv:2003.01102.
- [29] C. L. Edmunds, T. R. Tan, A. Milne, A. Singh, M. J. Biercuk, C. Hempel, “Scalable hyperfine qubit state detection via electron shelving in the $D_{5/2}$ and $F_{7/2}$ manifolds in $^{171}\text{Yb}^+$,” submitted (2020).
 - [30] K. Sugiyama, “Laser Cooling of Single $^{174}\text{Yb}^+$ Ions Stored in a RF Trap,” Japanese Journal of Applied Physics **38**, 2141 (1999).
 - [31] Y.-Y. Jau, J. D. Hunker, and P. D. D. Schwindt, “F-state quenching with CH_4 for buffer-gas cooled $^{171}\text{Yb}^+$ frequency standard,” AIP Advances **5**, 117209 (2015).
 - [32] S. Mulholland, H. A. Klein, G. P. Barwood, S. Donnellan, P. B. R. Nisbet-Jones, G. Huang, G. Walsh, P. E. G. Baird, and P. Gill, “Compact laser system for a laser-cooled ytterbium ion microwave frequency standard,” Rev. Sci. Ins. **90**, 033105 (2019).
 - [33] C. L. Edmunds, C. Hempel, R. J. Harris, V. Frey, T. M. Stace, and M. J. Biercuk, “Dynamically corrected gates suppressing spatiotemporal error correlations as measured by randomized benchmarking,” Phys. Rev. Research **2**, 013156 (2020).
 - [34] A. D. Ludlow, M. M. Boyd, J. Ye, E. Peik, and P. O. Schmidt, “Optical atomic clocks,” Rev. Mod. Phys. **87**, 637 (2015).
 - [35] W. F. Meggers, “The Second Spectrum of Ytterbium (Yb II),” Journal of research of the National Bureau of Standards. Section A, Physics and chemistry **71A**, 396 (1967).
 - [36] R. W. Berends, E. H. Pinnington, B. Guo, and Q. Ji, “Beam-laser lifetime measurements for four resonance levels of Yb II,” Journal of Physics B: Atomic, Molecular and Optical Physics **26**, L701 (1993).
 - [37] S. A. Webster, P. E. Blythe, K. Hosaka, G. P. Barwood, P. Gill, “Systematics shifts of the 467 nm electric octupole transition in $^{171}\text{Yb}^+$,” NPL Report CBTL M 31 (1999).
 - [38] P. Taylor, M. Roberts, G. M. Macfarlane, G. P. Barwood, W. R. C. Rowley, and P. Gill, “Measurement of the infrared $^2F_{7/2}-^2D_{5/2}$ transition in a single $^{171}\text{Yb}^+$ ion,” Phys. Rev. A **60**, 2829 (1999).
 - [39] P. Gill, H. A. Klein, A. P. Levick, M. Roberts, W. R. C. Rowley, and P. Taylor, “Measurement of the $^2S_{1/2}-^2D_{5/2}$ 411-nm interval in laser-cooled trapped $^{171}\text{Yb}^+$ ions,” Phys. Rev. A **52**, R909 (1995).
 - [40] N. Huntemann, M. Okhapkin, B. Lipphardt, S. Weyers, Chr. Tamm, and E. Peik, “High-Accuracy Optical Clock Based on the Octupole Transition in $^{171}\text{Yb}^+$,” Phys. Rev. Lett. **108**, 090801 (2012).
 - [41] H. A. Füst, C.-H. Yeh, D. Kalincev, A. P. Kulosa, L. S. Dreissen, R. Lange, E. Benkler, N. Huntemann, E. Peik, T. E. Mehlstäubler, “Coherent excitation of the highly forbidden electric octupole transition in $^{172}\text{Yb}^+$,” arXiv:2006.14356.
 - [42] Wayne M. Itano, “External-Field Shifts of the $^{199}\text{Hg}^+$ Optical Frequency Standard,” Journal of research of the National Institute of Standards and Technology **105**, 829 (2000).
 - [43] W. C. Martin and W. L. Wiese, “Atomic, Molecular, and Optical Physics Handbook,” National Institute of Standards and Technology. <http://physics.nist.gov/Pubs/AtSpec/index.html>.
 - [44] J. Vanier and C. Audoin, “The Quantum Physics of Atomic Frequency Standards,” Philadelphia : A. Hilger (1989).
 - [45] J. Wright, C. Auchter, C.-K. Chou, R. D. Graham, T. W. Noel, T. Sakrejda, Z. Zhou, and B. Blinov, “Toward a scalable quantum computing architecture with mixed species ion chains,” Quantum Information Processing **15**, 5339 (2016).
 - [46] I. V. Inlek, C. Crocker, M. Lichtman, K. Sosnova, and C. Monroe, “Multispecies Trapped-Ion Node for Quantum Networking,” Phys. Rev. Lett. **118**, 250502 (2017).
 - [47] Y. Wang, M. Um, J. Zhang, S. An, M. Lyu, J.-N. Zhang, L.-M. Duan, D. Yum, and K. Kim, “Single-qubit quantum memory exceeding \$10\$-minute coherence time,” Nat. Photonics **11**, 646 (2017).
 - [48] H. Knab, K. H. Knöll, F. Scheerer, and G. Werth, “Experimental ground state g_J -factor of Ba^+ in a Penning ion trap,” Z. Physik D Atoms, Molecules and Clusters **25**, 205 (1993).
 - [49] G. Marx, G. Tommaseo, G. and G. Werth, “Precise g_J - and g_I - factor measurements of Ba^+ isotopes,” Eur. Phys. J. D **4**, 279 (1998).
 - [50] M. Chwalla, K. Kim, T. Monz, P. Schindler, M. Riebe, C. F. Roos, and R. Blatt. “Precision spectroscopy with two correlated atoms,” Appl. Phys. B **89**, 483 (2007).
 - [51] C.-W. Chou, D. B. Hume, M. J. Thorpe, D. J. Wineland and T. P. Rosenband, “Quantum coherence between two atoms beyond $Q = 10^{15}$,” Phys. Rev. Lett. **106**, 160801 (2011).
 - [52] T. R. Tan, R. Kaewuam, K. J. Arnold, S. R. Chanu, Zhiqiang Zhang, M. S. Safronova, and M. D. Barrett, “Suppressing Inhomogeneous Broadening in a Lutetium Multi-ion Optical Clock,” Phys. Rev. Lett. **123**, 063201 (2019).
 - [53] D. J. Wineland, J. J. Bollinger, and Wayne M. Itano, “Laser-Fluorescence Mass Spectroscopy,” Phys. Rev. Lett. **50**, 628 (1983).